Cellulose Nanofibrils as reinforcing agents for PLA-based nanocomposites: an *in situ* approach

Stefano Gazzotti,[a, b, d] Riccardo Rampazzo,[a ,d] Minna Hakkarainen,[*, b] Daniele Bussini,[c] Marco Aldo Ortenzi,[a, d] Hermes Farina,[a, d] Giordano Lesma[a, d] and Alessandra Silvani[a, d]

[a] Department of Chemistry, Università degli Studi di Milano, Via Golgi 19, 20133 Milan, Italy

[b]Department of Fibre and Polymer Technology, KTH Royal Institute of Technology, 100 44 Stockholm, Sweden

[c]INNOVHUB-SSI Paper Department, Via Giuseppe Colombo 83, 20133 Milano, Italy

[d]CRC Materiali Polimerici "LaMPO", Department of Chemistry, Università degli Studi di Milano, Via Golgi 19, 20133 Milan, Italy

[*]Corresponding author: Minna Hakkarainen E-mail address: minna@kth.se.

Stefano Gazzotti. E-mail address: stefano.gazzotti@unimi.it.

Riccardo Rampazzo. E-mail address: riccardo.rampazzo@unimi.it.

Daniele Bussini. E-mail address: daniele.bussini@mi.camcom.it

Marco Aldo Ortenzi. E-mail address: marco.ortenzi@unimi.it.

Hermes Farina. E-mail address: hermes.farina@unimi.it.

Giordano Lesma. E-mail address: giordano.lesma@unimi.it.

Alessandra Silvani. E-mail address: alessandra.silvani@unimi.it.

Abstract

One-pot *in situ* polymerization approach was explored for the preparation of polylactide (PLA)-cellulose nanofibril (CNF) bio-nanocomposites. CNF were first prepared through enzymatic and mechanical treatment of bleached hardwood kraft pulp. The bio-nanocomposites- were then fabricated through ring opening polymerization (ROP) of L-lactide, in the presence of various amounts of fibrils. Molecular weight, thermal properties, surface morphology, mechanical and wettability properties of the PLA-CNF nanocomposites were evaluated. DSC analysis demonstrated the effect of CNF on crystallization and crystalline morphology of PLA. Improved modulus for the nanocomposites with respect to standard PLA was demonstrated, however, the differences in tensile stress were small probably due to the counteracting effects of reinforcement from CNF and the decreasing molecular weight as a function of CNF concentration. The absence of pulled-out fibers was assessed, highlighting the strong interface and covalent attachment of PLA chains on CNF surface. Finally, the covalent bonding of PLA chains on CNF surface was demonstrated by isolating the non-soluble part, consisting of PLA-grafted CNF, and characterization of this residue.

Keywords: A. Fibers; A. Nano composites; A. Polymers; A. Short-fibre composites; B. Interfacial strength

1. Introduction

Industrial interest around Polylactide (PLA) as a promising environmentally friendly alternative to oil-derived plastics is continuously increasing. In 2012 the world production of PLA was quantified as 180,000 tons, but according to estimates, it could rise to 800,000 tons by 2020.[1] Today one large research goal is to improve the chemical, physical and mechanical properties of PLA, in order to fully exploit its potential. To fill the performance gaps one of the most investigated approaches is the preparation of *nanocomposites*, i.e. composite materials consisting of nanometric size additives dispersed within a polymeric matrix leading potentially to improvement of e.g. thermal and mechanical properties of the final material.[2, 3] The nanometric size coupled with the high area to volume ratio, provides huge interface between the particle

itself and the polymeric matrix. When good interfacial interaction and proper dispersion of the filler into the polymer is reached, the newly formed material can exhibit significantly improved properties, that couldn't be achieved with larger scale particulate reinforcements, at least not on the same low level of filler material.

Many PLA-based nanocomposites have been prepared and described. Among them, the best results have been obtained with carbon nanotubes,[4] montmorillonite,[5-8] nanosilica[9] and carbon dots.[10] Aiming to produce fully organic *bio*-nanocomposites, we recently considered cellulose nanocrystals (CNC) as biocompatible, biodegradable and renewable additives with strong properties useful for increasing the performance of the final PLA-nanocomposite.[11,12] An *in situ* melt polymerization approach was described for the preparation of PLA-CNC nanocomposites. The exploitation of free -OH groups on CNC surface as initiators for the ring opening polymerization (ROP) of lactide resulted in an optimal compatibilization between the two phases. Final materials showed a considerable improvement in thermal and rheological properties with respect to standard PLA and conventional PLA-CNC nanocomposites.[13]

Aiming at further exploring the potential of an *in situ* approach for the preparation of a new generation of nanocomposites, the use of cellulose nanofibrils (CNF) as fillers is of interest. CNF are described as an aggregation of 10-50 cellulose elementary fibrils, showing extremely high Young modulus (~140 GPa), high aspect ratio and large surface area.[14-16] These properties make them ideal candidates as strengthening agents for polymeric materials. They can be extracted from almost all cellulose sources, e.g. wood,[17] hardwood and softwood pulps,[18] cotton fibers,[19] banana peel,[20] cassava root bagasse and peelings,[21] waste papers[22] and many others sources, through mechanical defibrillation, making them valuable also from an environmental point of view.

Given their green nature coupled with outstanding mechanical properties, CNF can be considered as one of the most promising reinforcing agents for the preparation of PLA-based bionanocomposites.[23] Common

PLA-CNF nanocomposite preparation methodologies rely on either melt blending[24] or solution casting.[25] These preparation strategies suffer from the strong difference in polarity between CNF and PLA, that makes the dispersion of the filler inefficient.[26, 27] For this reason, many different cellulose functionalization approaches were developed, in order to improve the compatibility between the two phases. Surface silylation,[28, 29] esterification[30, 31] and amination[32] are some of the most investigated reactions. Surface modification reaction prior to dispersion usually offers good results in terms of compatibilization but requires additional synthetic steps that could in principle damage the crystalline integrity of the fibers. In addition, the use of additional chemicals required for functionalization reactions could be negative from the environmental point of view. The application of an "one pot" approach, such as *in situ* synthesis, would therefore be highly advantageous from an environmental point of view and could, in principle, end up in an optimal interface between CNF and PLA. In particular, the free surface hydroxyl groups on CNF could be exploited as initiators in the ring opening polymerization (ROP) of lactide. This would result in a direct functionalization of CNF with PLA chains, anticipated to result in strong interface and good dispersion of the filler within the PLA matrix.

2. Materials and methods

2.1. Chemicals and Materials

The bleached hardwood kraft pulps used as raw materials for CNF production were kindly supplied by Innovhub (Milan; Italy). Endo-1,4-β-D-glucanase (*FiberCare R*) was purchased from Novozymes Italia S.r.l. (Monza; Italy) and L-lactide was purchased from Corbion (Gorinchem; Netherlands). All other chemicals including tin (II) 2-ethylhexanoate, 92.5-100 %; chloroform ($CHCl_3$), $\geq$ 99.5 %; dichloromethane (CH_2Cl_2, DCM), $\geq$ 99.8 % were purchased by Sigma-Aldrich and used as received.

2.2. CNF extraction

In accordance with UNI EN ISO 5264-2:2011, bleached hardwood kraft pulps were initially mildly treated until achieving 25-30 °SR level of freeness with a lab PFI mill. The obtained cellulose pulp was then

subjected to an enzymatic treatment by using *FiberCare R* type enzyme, an endoglucanase able to hydrolyze the 1,4 β-D-glycosidic bonds of cellulose. The enzymatic reaction was conducted in a reactor equipped with elix shaft at 50°C for 1h. The enzyme dosage was 0.1 kg/ton. Final part of the enzymatic treatment was a further refining of the cellulose pulp in order to achieve level of freeness around 75-80 °SR, which represents the maximum limit of refining obtainable with lab equipment. Cellulose pulp water dispersed with 2 % w/w fiber concentration was subjected to 7 homogenization cycles. The first 3 cycles were subjected to a different pression each one (500, 1000, 1300 bar) follow by the last 4 cycles with 1500 bar as a level of pressure. CNF dispersion obtained at the end of the treatment had a solid concentration of approximately 2 % w/w.

2.3. Synthesis of PLA

PLA was synthesized from L-lactide in bulk according to the following procedure. L-lactide (25 g) and tin octanoate (0.3 % w/w on lactide), added as a catalyst, were introduced in a 250 mL three necked round bottomed flask. Slow nitrogen flow was used to ensure the presence of inert atmosphere during the polymerization reaction. Mechanical stirring was provided (40 rpm). Reaction was conducted in a closed oven at 180 °C for 1 hour. At the end of the reaction, the polymer was left to cool overnight under nitrogen atmosphere.

2.4. Synthesis of PLA-CNF nanocomposites

Nanocomposites were synthesized by *in situ* polymerization, from L-lactide in bulk according to the following procedure. CNF were put in a three-necked round bottomed flask and dispersed in 50 mL of acetone under vigorous stirring and ultrasound treatment. This procedure ensured the disaggregation of the lyophilized fluffy CNF mass into single fibrils. 25 g of L-lactide was then added and left under stirring until complete dissolution. Acetone was evaporated using nitrogen flux and the reaction mixture was heated to 70 °C under vacuum in a closed oven for 2 hours in order to remove any residual moisture. After this drying step, reaction was performed following the procedure described for the synthesis of PLA. Plain

PLA and four nanocomposite samples with percentage of CNF 0, 0.1, 0.25, 0.5 and 1.0 % w/w were prepared and named as PLA, NC1, NC2, NC3 and NC4, respectively.

2.5. Differential scanning calorimetry (DSC)

Mettler-Toledo 820 was utilized to conduct the measurements. 5 mg of each sample was placed in a 100 μl aluminium cup with a pinhole on the lid. The applied heating rate was 10 °C min^{-1} in a nitrogen atmosphere (rate 50 ml min^{-1}). Thermal behaviour of the samples was investigated using the following temperature cycles: First heating from 25 °C to 200 °C, then kept 5 min isothermally at 200 °C, cooling from 200 °C to 25 °C and kept 2 min isothermally at 25 °C. This was followed by second heating from 25 °C to 200 °C. The first heating and cooling, were run to eliminate residual internal stresses deriving from the synthesis. Glass transition temperature (T_g), cold crystallization temperature (T_{cc}) and melting temperature (T_m) were determined from the second heating curve.

2.6. Thermogravimetric analysis (TGA)

Mettler-Toledo TGA/SDTA 851e was utilized for thermal analysis. 5 mg of each sample was placed into a 70 μl alumina cup and heated at a rate of 10 °C min^{-1}. The measurements were performed under 80 ml min^{-1} nitrogen flow.

2.7. Size exclusion chromatography (SEC)

Verotech PL-GPC 50 Plus system equipped with a PL-RI Detector and two PLgel 5 μm MIXED-D (300 x 7.5 mm) columns from Varian were employed for the measurements. Chloroform was used as the mobile phase (1 ml/min, 30 °C) and toluene as an internal standard to correct for flow rate fluctuations. The calibration was based on polystyrene standards with a narrow molecular weight ranging from 160 to 371 000 g/mol. Samples solutions were filtered on 0.45 μm filters before the analysis. Molecular weight data therefore refers only to the soluble part that went through the filter pores.

2.8. Tensile testing

The testing was conducted on an INSTRON 5944 module equipped with pneumatic grips. A 500 N load cell was used for the measurements with a gauge length of 10 mm, and a crosshead speed of 5 mm/min was applied. The samples were cut into strips of width 0.5 cm with a thickness of an average of 0.1 mm. Before analysis, the test strips were preconditioned according to ASTM D618–96 (40 h at 50 % ± 5 % relative humidity and 23°C ± 1 °C).

2.9. Fourier-transform infrared spectroscopy (FT-IR)

FT-IR Spectrometer (Spectrum 100, PerkinElmer) with an attenuated total reflection (ATR) was used to register spectra for PLA, all nanocomposites and CNF alone.

2.10. Water contact angle

Wettability of the PLA/CNF films with different % of CNF (0, 0.1, 0.25, 0.5) were determined by measuring static contact angles (θ) of polar Milli-Q water (18.3 MΩ cm) using a KSV Instruments LTD CAM 200 contact angle meter. All the static contact angles were determined by using sessile drop method at room temperature (23 °C; $\approx$ 40% RH) on four different positions for each sample by dropping 3 ± 0.5 μL of liquid onto the substrate. The contact angle values (θ) were detected 5 s after the deposition of water droplet onto the sample. Statistical analysis experimental data were analyzed using a one-way analysis of variance (ANOVA) conducted using Statgraphics® S-plus 5.1 as statistical software, assuming p-value $\leq$ 0,05.

2.11. Scanning electron microscopy (SEM)

SE- 4800 SEM (Hitachi, Japan), operating at a low accelerated voltage of 0.5 keV to avoid damaging the matrix, was utilized to characterize the films. Prior to SEM observation, all samples were sputter-coated with a 3.5 nm-thick gold layer. For additional SEM observations of the sample morphology, the PLA and NC4 films were etched in a water−methanol (1:2, v:v) solution containing 0.025 mol/L of sodium hydroxide and 1 mol/L of sodium chloride for 16 h at 10 °C.

2.12. Film casting

Films for SEM analyses and tensile testing were obtained by casting from a chloroform solution. 2 grams of polymer was dissolved into 30 mL of $CHCl_3$ at 30 °C. The solution was cast on a glass surface and the solvent was evaporated at room temperature and pressure overnight. Films were then kept in vacuum at 25 °C for three days. Complete evaporation of the solvent was checked through TGA analysis.

2.13. Isolation of CNF

CNF from the nanocomposites was isolated through centrifugation process as indicated: ≈ 1 g of sample (PLA, NC1, NC2, NC3 and NC4) was dissolved in 50 ml of DCM and centrifuged at 4000 rpm for 10 minutes. This operation was repeated three times for each sample, removing each time the liquid part, in order to completely remove the soluble species. Residue consisting of CNF and CNF bound PLA was then dried in vacuum oven at room temperature until constant weight was reached. Quantity of PLA bounded to CNF surface was determined as ratio between the weight of the grafted PLA and theoretical weight of CNF introduced in the feed.

3. Results and discussion

The efficacy of an *in situ* polymerization approach for the synthesis of cellulose nanofibril-containing PLA-based nanocomposites was demonstrated. Several nanocomposites were synthesized, with increasing concentration of CNF in the feed. Properties of the resulting materials were studied and the effect of different CNF concentrations investigated. Cellulose nanofibrils were also isolated after the reaction and characterized, demonstrating the presence of PLA grafted onto the surface.

3.1. Synthesis of nanocomposites

Nanocomposites were synthesized through an *in situ* polymerization reaction with different concentrations of CNF in the feed. The aim was to exploit the free OH groups on CNF surface as initiators for the ROP of L-lactide to directly functionalize the surface of the fibrils by "grafting-from" approach. The covalent bond

8

between the nanofibrils and PLA-grafts is expected to lead to effective compatibilization between the nanofiller and the polymer matrix. A schematic representation of the reaction is shown in **Fig. 1**. The product of the reaction was expected to be a complex mixture of species including both PLA chains bounded to CNF surface, as represented in **Fig. 1**, as well as free PLA chains. These free chains can be analyzed through SEC analysis and they also give an indication of the length of the PLA chains grafted on the surface of CNF.
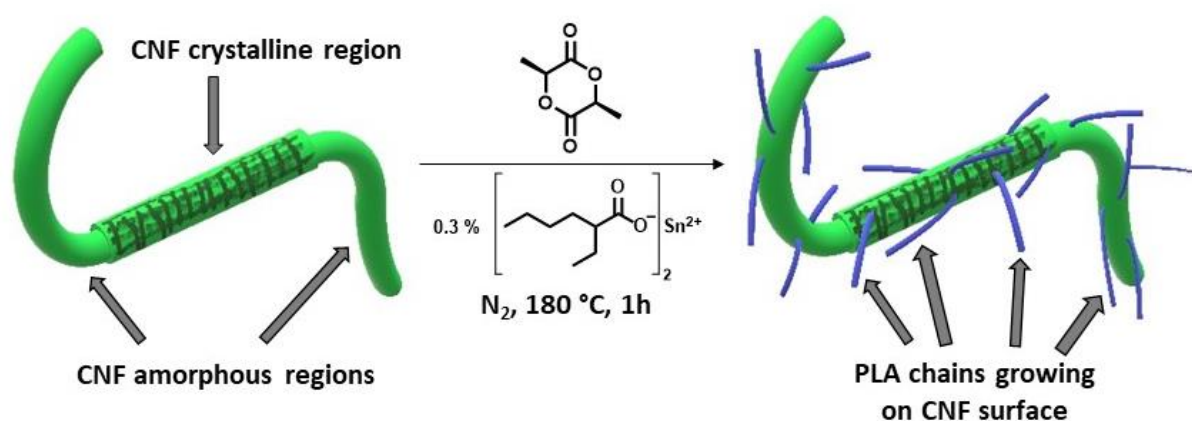

Fig. 1. Schematic representation of the "grafting-from" reaction resulting in PLA chain growing from the CNF surface.

3.2. Molecular weight determination

SEC analyses were performed in order to determine the effect of CNF concentration on the reaction outcome in terms of molecular weights of the synthesized PLA chains. The results are reported in **Tab. 1**.

Tab. 1. The molecular weight of the PLA chains with increasing concentration of CNF. The molecular weights were determined against PS calibration.

Sample	CNF (wt %)	$\overline{M_n}$ (g mol^{-1})	$\overline{M_w}$ (g mol^{-1})	Đ
PLA	0	284 000	384000	1.4
NC1	0.1	247 000	351000	1.4
NC2	0.25	212 000	294000	1.4
NC3	0.5	106 000	153000	1.4
NC4	1	54000	74000	1.4

Molecular weight data show a steady decrease of the molecular weight as a function of increasing CNF concentration in the feed (see Fig. 2). This is in good agreement with the hypothesis and expectation that the free -OH groups on CNF surface act as initiators for the ROP of lactide. Increasing the CNF concentration, thus, resulted in an increased initiator concentration, which further resulted in larger number of PLA chains initiated leading to decreased average molecular weight. Differences were already detectable between NC1 and NC2 samples and it appears that going from NC2 to NC3 as the concentration of CNF doubles, the molecular weight of the product decreases by half. Similar behavior and further halving is observed going from NC3 to NC4.
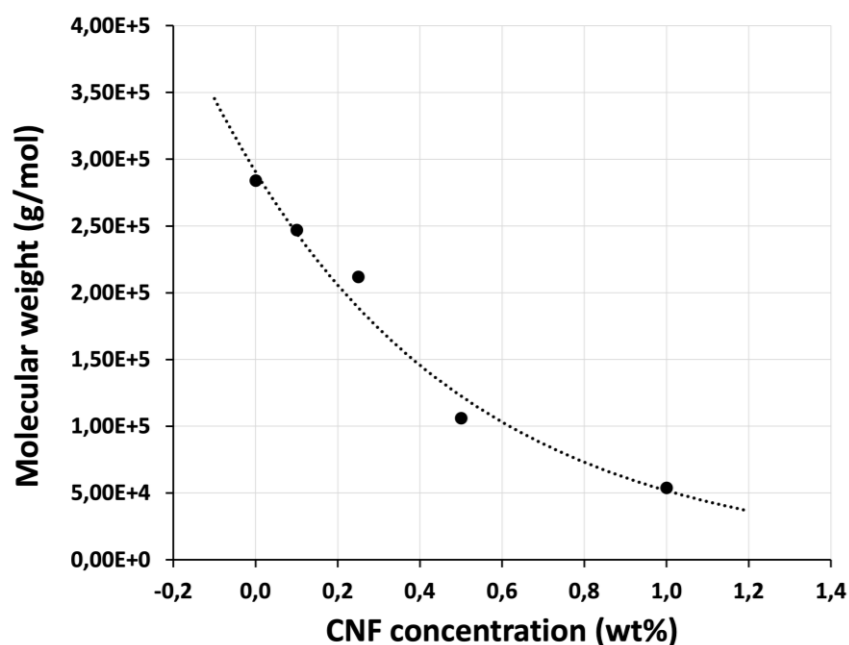

Fig. 2. Molecular weight as a function of increasing CNF concentration.

3.3. Thermal properties

The thermal stability of the composites and PLA were investigated by TGA and the degradation data for all the materials are reported in **Tab. 2** with temperatures relative to 5 % ($T_{5\%}$), 50 % ($T_{50\%}$) and 95 % ($T_{95\%}$) weight loss. No significant differences were detectable among all the nanocomposites nor in comparison with the plain PLA sample.

Tab. 2. $T_{5\%}$, $T_{50\%}$ and $T_{95\%}$ from TGA for all the samples.

Sample	$T_{5\%}$	$T_{50\%}$	$T_{95\%}$
PLA	242.4	285.0	309.1

NC1	242.0	279.2	306.3
NC2	236.7	283.4	309.3
NC3	237.9	283.2	309.1
NC4	234.8	284.1	309.7

The influence of CNF on the thermal properties and crystallinity was evaluated by DSC. The DSC thermograms related to second heating scan for all the samples are reported in **Fig. 3**, together with an expansion of the first heating scan in the melting peak region. Complete thermograms for all samples are reported in the SI file.
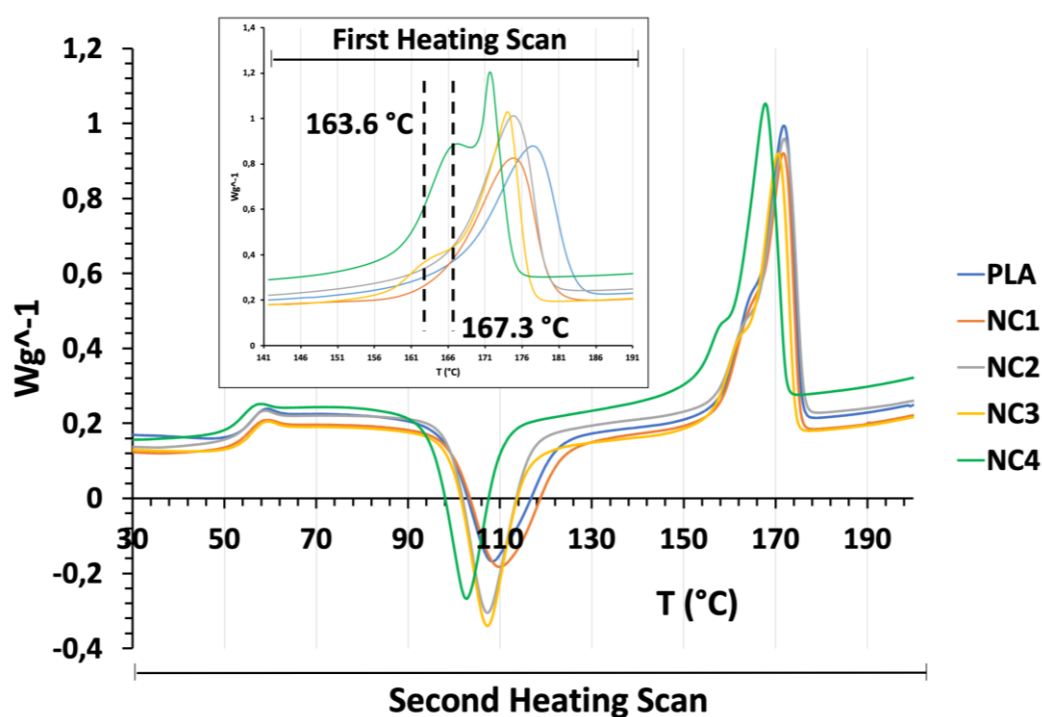

Fig. 3. DSC thermograms illustrating the second heating scan as well as an expansion of the first heating scan in the melting peak region.

Tab. 3. Thermal properties and crystallinity data for all samples.

Sample	First Heating Scan			Second Heating Scan		
	T_g	T_m	χ_c	T_{cc}	T_m	χ_c
PLA	54.5	177.8	57.5	108.4	171.8	6.2
NC1	53.7	174.2	52.7	110.0	171.7	4.2
NC2	53.6	175.2	50.8	107.2	171.9	2.9
NC3	54.3	174.2	53.6	107.2	170.7	5.1

NC4	52.6	171.8	65.3	102.7	167.8	10.0

Thermal characteristics from the DSC thermograms from both first and second heating scans are reported in **Tab. 3**. The thermal behavior of the samples, aside the glass transition temperature (T_g), is affected by the concentration of CNF, which particularly influenced the crystallinity of the samples. It has been reported that for classical PLA-CNF nanocomposites, prepared through post-polymerization solution mixing, there are two observed influences. In particular, at low concentrations ($\leq$ 1 wt %) the addition of CNF promoted the crystallization.[33] On the other hand, at higher concentrations (10 wt %) the nanofibrils had detrimental effect on crystallization behavior of PLA.[34] These results were attributed to the large CNF aspect ratio as well as to the entanglements that restricted the conformational freedom of PLA chains which is necessary for efficient organization in ordered crystals. As the DSC data in **Tab. 3** shows, the synthesized samples were characterized by a peculiar trend that can be related to the previous observations. In particular, there is a decrease in degree of crystallinity going from PLA to NC1 and NC2 samples. Then, the crystallinity again increases for NC3 and reaches the highest value among the studied materials for NC4. In order to explain this trend, the covalent bond between CNF and PLA, could reduce the mobility of the chains, hindering the crystallization. Since several PLA chains can be attached to one CNF, the total molecular weight of these grafted products can be multiple to the values reported in **Tab. 3**, which will also increase the number of entanglements and could further decrease the chain mobility. However, as the concentration of fibrils increased, the molecular weight of the PLA-grafts decreased, which probably promoted the crystallization process. This hypothesis fits well with thermal data relative to NC4 sample, which also clearly exhibited the lowest cold crystallization temperature among all samples, indicating a higher tendency to crystallize. Although the actual degrees of crystallinity are very different from the first and second heating scan, due to the low crystallization rate of PLA, the same degree of crystallinity trend can be observed during the first and second heating scans. In addition, during the first heating scan, NC4 sample and to some degree NC3 show a bimodal melting peak, as highlighted by the expansion in **Fig. 3**. In particular, the melting transition of NC3 is characterized by a small shoulder at 163.6 °C, in addition to the main melting peak at 174.2 °C, while NC4 appears to have two clear melting peaks at 167.3 °C and 171.8 °C.

The other materials, PLA, NC1 and NC2, have single melting peaks at temperature range 174.2-177.8 °C. This behavior can be explained by the formation of two different crystalline phases. PLA can either crystallize in a well-ordered α crystalline phase as well as in a less ordered α' structure. α' crystals form as disordered counterparts of α crystals with lower melting temperature as compared to α crystals.[35] Their presence in these samples could be explained by the high concentration of CNF possibly both acting as nucleation agents and causing some prevention of chain movement due to the covalent attachment, which could lead to less ordered crystal structure.

3.4. Morphological characterization by SEM

The film surfaces were also characterized through SEM analyses to evaluate how CNF affects the surface morphology of the films. The difference in polarity between CNF and PLA has been described as the biggest hurdle for an efficient dispersion of the filler. For this reason, different compatibilization reactions have been described with the aim of improving dispersibility.[28-32] Here the covalent attachment between PLA chains and CNF should effectively improve the dispersion of CNF. SEM micrographs of films' surface are reported in **Fig. 4**.
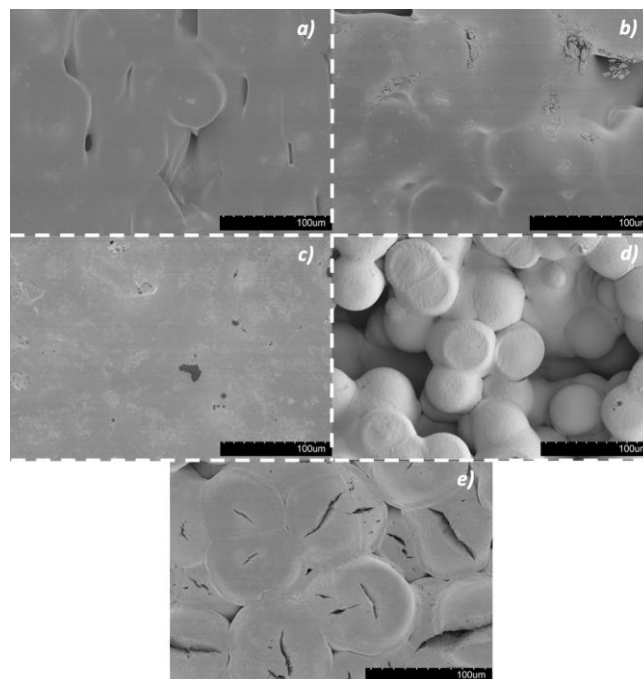

Fig. 4. SEM micrographs for *a)* PLA, *b)* NC1, *c)* NC2, *d)* NC3, and *e)* NC4.

Samples showed significantly different surfaces, depending on the CNF concentration. In particular, the observed surface morphologies correlated with the degree of crystallinity of the films determined through DSC analyses from the first heating scan. Round spherulite crystal structures became less and less visible going from PLA to NC2. **Fig. 4c** shows an almost completely flat surface of NC2, which had the lowest crystallinity degree among all synthesized polymers. NC3 product was characterized by a highly irregular surface, with well defined, round spherulite type structures. Finally, NC4 illustrated again spherulite type structures on the surface of the films. Etching process was conducted on PLA and NC4 samples, in order to remove the amorphous parts and better expose the crystalline structure of the materials. Micrographs of the etched samples are reported in **Fig. 5**.
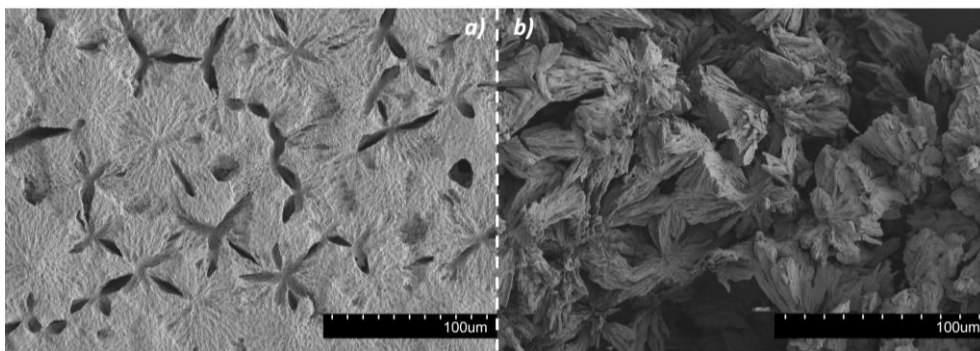

Fig. 5. SEM micrographs of *a)* etched PLA sample and *b)* etched NC4 sample.

The etched samples showed clear differences in crystalline patterns between the two samples. Standard PLA appears to have a much more regular disposition of crystal lamellae in more planar spherulite structures. In NC4 nanocomposite crystallites were significantly more exposed after the etching, probably due to the lower molecular weight of the polymer. Their spatial arrangement seems less ordered and they are growing in more tridimensional manner. Even if it was not possible to fully observe CNF embedded in the matrix, it can be assumed that they had a strong effect in defining these clearly different morphologies of the final material, as already reported in literature.[34] The significant differences among samples surfaces can be attributed to the differences in crystallization behavior, promoted by the combined effect of molecular weight lowering and CNF concentration increase.

3.5. Tensile testing

Tensile testing was performed to evaluate the effect of CNF on the mechanical properties of the synthesized nanocomposites. However, the testing of NC4 film was not possible due to the brittleness of the material. The results for PLA, NC1, NC2 and NC3 are reported in **Tab. 4.** An increased brittleness and decreased tensile strain were detected with increasing concentration of CNF, while Young's modulus shows a significant increase as a function of CNF concentration (maximum increase $\approx$ 37%).

Tab. 4. Mechanical properties of the synthesized samples.

Sample	Young's Modulus [GPa]	Tensile strain at break [%]	Tensile stress at break [MPa]
PLA	1.9 ± 0.1	40.6 ± 0.7	23.7 ± 0.6
NC1	2.2 ± 0.1	11.8 ± 0.6	24.8 ± 0.8
NC2	2.2 ± 0.2	5.5 ± 0.3	23.0 ± 0.9
NC3	2.6 ± 0.2	2.2 ± 0.2	21.0 ± 0.6

Literature data report a strengthening effect of CNF in PLA/CNF nanocomposites, given the outstanding mechanical strength of nanofibrils.[36] In particular, previous reports of such nanocomposites prepared through solvent casting demonstrate an increase of both modulus and tensile strength. As data reported in **Tab. 4** show, tensile stress at break of NC1 and NC2 is quite similar to that of PLA, while slight decreases is noticed for NC3. In order to explain this behavior, the molecular weight of the matrix has to be considered. To this regard, it was reported that the decrease of molecular weight of pure PLA has detrimental effect on material's mechanical properties.[37] In addition, lower molecular weight matrices in nanocomposites lead to a significant decrease in tensile strength of the final material.[38, 39] That said, considering the great difference in molecular weight between PLA and NC3 samples (> 50%), the small decrease registered still appears as a promising result. With increasing concentration of CNF in the feed, the material becomes

stiffer, resulting in a consistent decrease in strain at break. The stiffening effect of CNF in many different
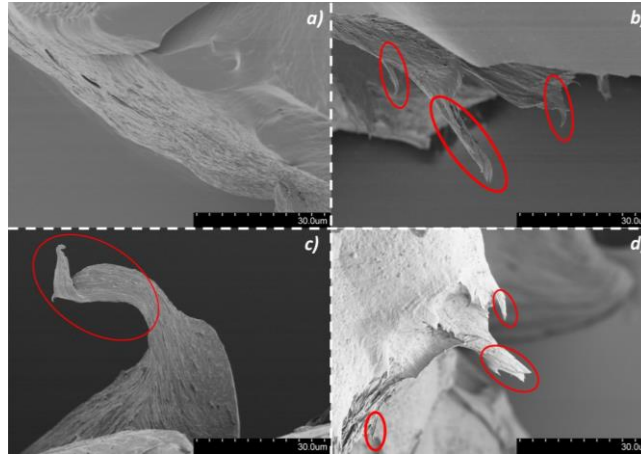
polymeric matrices has been widely discussed.[40-43]

Fig. 6. SEM images of the tensile-fractured surfaces of *a)* PLA, *b)* NC1, *c)* NC2, *d)* NC3.

The tensile-fractured surfaces were examined by SEM, in order to determine the possible presence of

pulled-out fibers, see **Fig. 6**. Samples showed clearly different morphologies depending whether cellulose

nanofibers were present or not. In particular, the fracture surface for PLA sample appears to be smooth

and regular. On the other hand, NC1, NC2 and NC3 samples are characterized by the presence of

protruding regions that are likely attributable to PLA-covered fibers. During the mechanical stress, CNF can

act as bridging species between the two halves of the breaking specimen and remain exposed after

breakage. This bridging action of CNF is highlighted in **Fig. 7** on a non-completely broken surface of NC2

sample. None of the analyzed samples show signs of pulled-out fibers. This is a good indicator of the

efficiency of the applied synthetic methodology, which results in strong interface between the filler and the

matrix. In particular, as reported by Qian et al.,[44] the increase in compatibility between the two phases is

highlighted by the appearance of elongated protruding species in the direction of tension, which are not

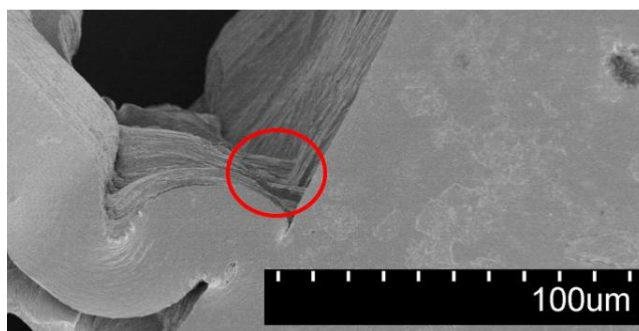present for pure PLA specimens.

Fig. 7. An example of the bridging effect CNF in NC2 sample.

3.6. Water contact angle measurements

The water contact angle measurements were performed on PLA, NC1, NC2 and NC3 films, since NC4 was

too brittle to obtain a good film. Static water contact angle values are reported in **Tab. 5**.

Tab. 5. Water contact angle values for the analyzed samples.

Sample	Static contact angle (θ)
PLA	69.4 ± 4.0^a
NC1	69.2 ± 3.6^a
NC2	74.3 ± 2.3^a
NC3	53.1 ± 0.4^b

PLA, NC1 and NC2 samples didn't show significant differences ($p \leq 0.05$) in terms of wettability. The surface

of NC3, however, had clearly lower contact angle value, indicating more wettable surface as compared to

the other materials tested. FT-IR of the film surfaces (reported in the SI file) showed an -OH absorption

band with higher intensity for nanocomposites in comparison to PLA. However, this difference could not be

explanatory for the trend observed for water contact angle values. For this reason, it is reasonable to

assume that these differences arise mainly from the significantly different surface topography, especially

for NC3 described through SEM micrographs. In addition, NC2 had the most planar or smooth surface,

which might explain the slightly higher contact angle value as compared to PLA and NC1.

3.7. Isolation of CNF with grafted PLA

CNF with grafted PLA chains were isolated from the free PLA chains through centrifugation protocol

described in the experimental section. In **Tab. 6** the weight of the residue isolated through centrifugation is

reported (residue weight) and compared to the theoretical CNF content in the sample, considering the initial loading of nanofibrils before the reaction. Weight of PLA grafted per milligram CNF was then been calculated as the ratio between the grafted PLA and the theoretical weight of CNF added. It appeared as a general trend that the more CNF in the feed, the less PLA is bounded to their surface. This observation is consistent with the observed values for molecular weight detected via SEC. As the concentration of CNF increases the length of the grafted chains decreases, due to the higher quantity of initiating species in the feed. The isolated products were also characterized through FTIR spectra, which are reported in **Fig. 8**.

Tab. 6. The weight of CNF, CNF-grafted and free PLA as well as the amount of PLA grafted per milligram CNF. The values were normalized to 1 g of sample.

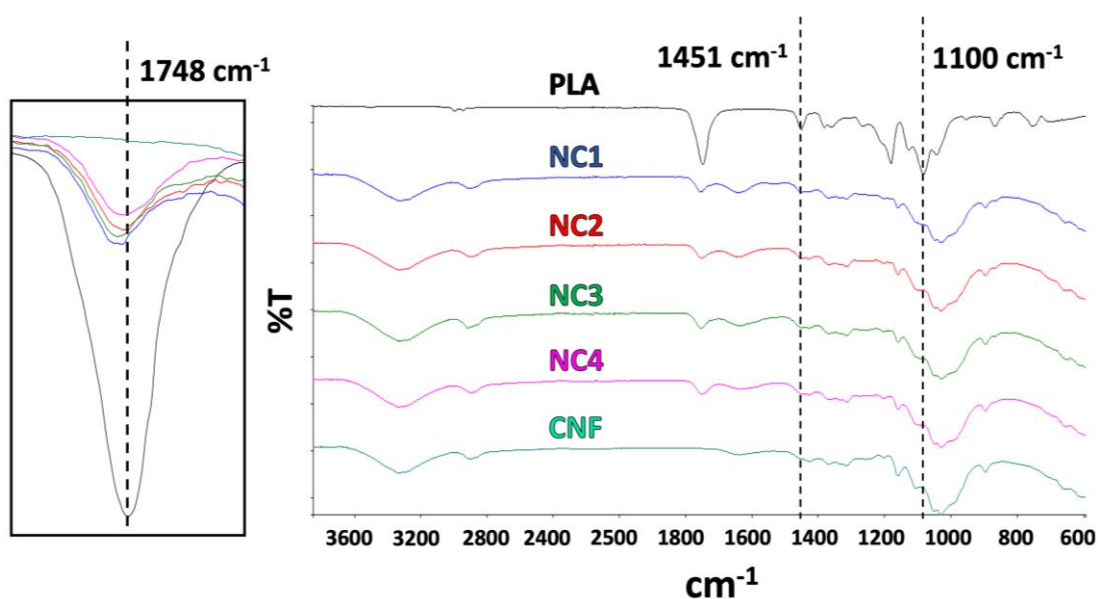| Sample	Theoretical CNF weight (mg)	Residue weight (CNF+CNF grafted PLA) (mg)	Soluble part (free PLA) (mg)	PLA grafted to CNF (mg PLA/mg CNF)
PLA	0	0	1	0
NC1	1.0	79	921	78
NC2	2.5	82	918	32
NC3	5.0	222	778	43
NC4	10.0	219	781	21

Fig. 8. FT-IR spectra of PLA; CNF and the products isolated after centrifugation.

The spectra of the products isolated by centrifugation closely resembled the spectrum of CNF, therefore indicating the clear presence of CNF in these residues. As expected PLA-related signals were also be clearly detected. In particular, signals at 1451 and 1100 cm^{-1} are detected only for PLA and its nanocomposites. Even more evident is the band around 1750 cm^{-1} related to the carbonyl groups in PLA. As magnification in **Fig. 8** shows, intensity of this carbonyl group signal in the nanocomposites follows the same trend observed for weight residues, confirming the different quantities of surface-bound PLA.

SEM images showing a comparison between starting CNF and isolated residue after centrifugation of sample NC4 are reported in **Fig. 9**.
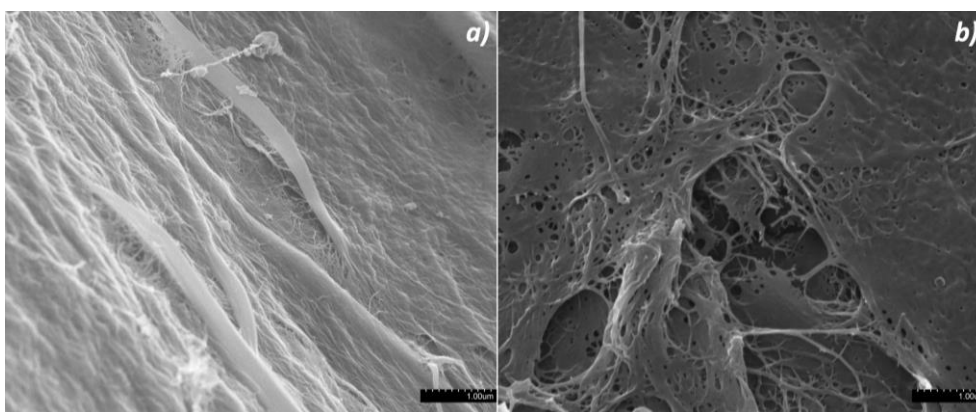

Fig. 9. SEM comparison between a) neat CNF and b) isolated residue after centrifugation of sample NC4.

Fig. 9a shows the presence of fibrous aggregates as well as free fibers. These aggregates are not more visible after the reaction (**Fig. 9b**), further indicating good dispersion of CNF within the matrix. In addition, isolated fibers after centrifugation appear embedded in the polymer, demonstrating the strong connection between the two phases. To this regard, in the case the two phases were not covalently bounded, the repeated DCM centrifugation steps would've ended up in the complete removal of soluble PLA. The presence of PLA-related bands in the FT-IR spectra of the isolated residues demonstrates the actual presence of CNF-covalently bounded PLA chains.

4. Conclusions

One-pot *in situ* approach was successfully exploited for the synthesis of PLA-CNF nanocomposites. Different samples containing different quantities of fibrils were synthesized and the effects on the properties of the resulting materials studied accordingly. Exploiting free -OH groups as initiators in lactide ROP, the increase of CNF in the feed resulted in a decrease of the molecular weight of the product. The presence of the fillers did not have noticeable effect on the thermal stability of the products, but their crystallization behavior and crystalline morphology was affected. It appeared that the dimensions and shape of crystallites could be correlated with the differences in crystallinity degree and melting temperatures observed through DSC analysis. Tensile tests proved an increased Young's modulus even with the decrease of the molecular weight. On the other hand, higher concentrations of CNF resulted in more brittle materials. Finally, the covalent bond between CNF and PLA chains was demonstrated, through isolation and analysis of the reacted fibrils. As the increase of CNF concentration decreases the molecular weight of the final polymer, the protocol here presented could be suitable as PLA-CNF compatibilization strategy. Very high CNF loadings in the feed would eventually end up in very short PLA chains. However, the covalent bond between CNF surface and the polymer allows for an optimal interaction between the phases and therefore could be useful in further dispersion procedures.

References

[1] M. Karamanlioglu, R. Preziosi, G. D. Robson, Abiotic and biotic environmental degradation of the bioplastic polymer poly(lactic acid): A review, Polym. Degrad. Stab. 137 (2017) 122-130.

[2] A. J. Crosby, J. Y. Lee, Polymer Nanocomposites: The "Nano" Effect on Mechanical Properties, Polym. Rev. 47 (2007) 217–229.

[3] G. Armstrong, An introduction to polymer nanocomposites, Eur. J. Phys. 36 (2015) 063001.

[4] A. Akbari, M. Majumder, A. Tehrani, Polylactid acid (PLA) Carbon nanotubes composites. Handbook of Polymer Nanocomposites. Processing, Performance and application. (2015) DOI: 10.1007/978-3-642-45229-1_45.

[5] M. Pluta, A. Galeski, M. Alexandre, M. A. Paul, P. Dubois, Polylactide/Montmorillonite nanocomposites and microcomposites prepared by melt blending: structure and some physical properties, J. Appl. Polym. Sci. 86 (2002) 1497-1506.

[6] P. Gelineau, S. Weigand, L. Cauvin, F. Bedoui, Compatibility effects of modified montmorillonite on elastic properties of nano-reinforced Poly(lactid acid): Experimental and modeling study, Polym. Test. 70 (2018) 441-448.

[7] K. Fukushima, A. Fina, F. Geobaldo, A. Venturello, G. Camino, Properties of poly(lactid acid) nanocomposites based on montmorillonite, sepiolite and zirconium phosphonate, Express Polym. Lett. 6 (2012) 914-926.

[8] M. A. Ortenzi, L. Basilissi, H. Farina, G. Di Silvestro, L. Piergiovanni, E. Mascheroni, Evaluation of crystallinity and gas barrier properties of films obtained from PLA nanocomposites synthesized via "in situ" polymerization of L-lactide with silane-modified nanosilica and montmorillonite, Eur. Polym. J. 66 (2015) 478-491.

[9] L. Basillissi, G. Di Silvestro, H. Farina, M. A. Ortenzi, Synthesis and characterization of PLA nanocomposites containing nanosilica modified with different organosilanes II: effect of the organosilanes on the properties of nanocomposites: thermal characterization, J. Appl. Polym. Sci. 128 (2013) 3057-3063.

[10] H. Xu, L. Xie, J. Li, M. Hakkarainen, Coffee Grounds to Multifunctional Quantum Dots: Extreme Nanoenhancers of Polymer Biocomposites, ACS Appl. Mater. Interfaces 9 (2017) 27972-27983.

[11] F. V. Ferreira, A. Dufresne, I. F. Pinheiro, D. H. S. Souza, R. F. Gouveia, L. H. I. Mei, L. M. F. Lona, How do cellulose nanocrystals affect the overall properties of biodegradable polymer nanocomposites: a comprehensive review, Eur. Polym. J. 108 (2018) 274-285.

[12] E. Mascheroni, R. Rampazzo, M. A. Ortenzi, G. Piva, S. Bonetti, L. Piergiovanni, Comparison of cellulose nanocrystals obtained by sulfuric acid hydrolysis and ammonium persulfate, to be used as coating on flexible food-packaging materials, Cellulose 23 (2016) 779-793.

[13] S. Gazzotti, H. Farina, G. Lesma, R. Rampazzo, L. Piergiovanni, M. A. Ortenzi, A. Silvani, Polylactide/cellulose nanocrystals: The in situ polymerization approach to improved nanocomposites Eur. Polym. J. 94 (2017) 173–184.

[14] H. P. S. Abdul Khalil, A. H. Bhat, A. F. Ireana Yusra, Green composites from sustainable cellulose nanofibrils: A review, Carbohydr. Polym. 87 (2012) 963–979.

[15] K. Y. Lee, Y. Aitomäki, L. A. Berglund, K. Oksman, A. Bismarck, On the use of nanocellulose as reinforcement in polymer matrix composites, Compos. Sci. Technol. 105 (2014) 15–27.

[16] K. Oksman, Y. Aitomäki, A. P. Mathew, G. Siqueira, Q. Zhou, S. Butylina, S. Tanpichai, X. Zhou, S. Hooshmand, Review of the recent developments in cellulose nanocomposite processing, Compos. Part A Appl. Sci. Manuf. 83 (2016) 2–18.

[17] K. Abe, S. Iwamoto, H. Yano, Obtaining cellulose nanofibers with a uniform width of 15 nm from wood, Biomacromolecules 8 (2007) 3276-3278.

[18] W. Stelte, A. R. Sanadi, Preparation and characterization of cellulose nanofibers from two commercial hardwood and softwood pulps, I & E Chem. Res. 48 (2009) 11211-11219.

[19] E. M. T. Teixeira, A. C. Correa, A. Manzoli, F. Leite, C. R. Oliveira, L. H. C. Mattoso, Cellulose nanofibers from white and naturally colored cotton fibers, Cellulose 17 (2010) 595-606.

[20] H. Tibolla, F. M. Pelissari, J. T. Martins, A. A. Vicente, F. C. Menegalli, Cellulose nanofibers produced from banana peel by chemical and mechanical treatments: characterization and cytotoxicity assessment, Food Hydrocoll. 72 (2018) 192-201.

[21] A. L. M. P. Leite, C. D. Zanon, F. C. Menegalli, Isolation and characterization of cellulose nanofibers from cassava root bagasse and peelings, Carbohydr. polym. 157 (2017) 962-970.

[22] H. Takagi, A. N. Nakagaito, M. Shahrill, Extraction of cellulose nanofiber from waste papers and application to reinforcement in biodegradable composites, J. Reinf. Plast. Compos. 32 (2013) 1542-1546.

[23] Q. Ping, G. Yuan, W. Guo-feng, Z. Li-ping, Nanocomposites of poly(lactic acid) reinforced with cellulose nanofibrils, BioResources 5 (2010) 1811-1823.

[24] S. Yeng-Fong, C. Man-Yun, C. Wen-Chuan, L. Hong-Yuan, C. Chih-Ming, Completely biodegradable composites reinforced by the cellulose nanofibers of pineapple leaves modified by eco-friendly methods, J. Polym. Res. 24 (2016) 209.

[25] J. Trifol, D. Plackett, C. Sillard, P. Szabo, J. Bras, A. E. Daugaard, Hybrid poly(lactic acid)/nanocellulose/ nanoclay composites with synergistically enhanced barrier properties and improved thermomechanical resistance, Polym. Int. 65 (2016) 988–995.

[26] Y. Habibi, L. A. Lucia, O. J. Rojas, Cellulose Nanocrystals: Chemistry, Self-Assembly, and Applications, Chem. Rev. 110 (2010) 3479–3500.

[27] S. Fujisawa, T. Saito, S. Kimura, T. Iwata, A. Isogai, Surface Engineering of Ultrafine Cellulose Nanofibrils toward Polymer Nanocomposite Materials, Biomacromolecules 14 (2013) 1541–1546.

[28] C. Gousse, H. Chanzy, M.L. Cerrada, E. Fleury, Surface silylation of cellulose microfibrils: preparation and rheological properties, Polymer 45 (2004) 1569–1575.

[29] P. Qu, Y. Zhou, X. Zhang, S. Yao, L. Zhang, Surface Modification of Cellulose Nanofibrils for Poly(lactic acid) Composite Application, J. Appl. Polym. Sci. 125 (2012) 3084–3091.

[30] S. Ifuku, M. Nogi, K. Abe, K. Handa, F. Nakatsubo, H. Yano, Surface Modification of Bacterial Cellulose Nanofibers for Property Enhancement of Optically Transparent Composites: Dependence on Acetyl-Group DS, Biomacromolecules 8 (2007) 1973-1978.

[31] S. Berlioz, S. Molina-Boisseau, Y. Nishiyama, L. Heux, Gas-Phase Surface Esterification of Cellulose Microfibrils and Whiskers, Biomacromolecules 10 (2009) 2144–2151.

[32] Y. Lua, M. C. Cueva, E. Lara-Curzio, S. Ozcan, Improved mechanical properties of polylactide nanocomposites-reinforced with cellulose nanofibrils through interfacial engineering via amine-functionalization, Carbohydr. Polym. 131 (2015) 208–217.

[33] W. Ding, R. K. M. Chu, L. H. Mark, C. B. Park, M. Sain, Non-isothermal crystallization behaviors of poly(lactic acid)/cellulose nanofiber composites in the presence of CO_2, Eur. Polym. J. 71 (2015) 231–247.

[34] H. Yu, H. Zhang, M. Song, Y. Zhou, J. Yao, Q. Ni, From Cellulose Nanospheres, Nanorods to Nanofibers: Various Aspect Ratio Induced Nucleation/Reinforcing Effects on Polylactic Acid for Robust-Barrier Food Packaging, ACS Appl. Mater. Interfaces 9 (2017) 43920–43938.

[35] M. Di Lorenzo, R. Androsch, Stability and Reorganization of α'-Crystals in Random L/D-Lactide Copolymers, Macromol. Chem. Phys. 217 (2016) 1534–1538.

[36] Z. Ying, D. Wu, Z. Wang, W. Xie, Y. Qiu, X. Wei, Rheological and mechanical properties of polylactide nanocomposites reinforced with the cellulose nanofibers with various surface treatments, Cellulose 25 (2018) 3955–3971.

[37] G. Perego, G. Cella, C. Bastioli, Effect of Molecular Weight and Crystallinity on Poly(lactic acid) Mechanical Properties, J. Appl. Polym. Sci. 59 (1996) 37-43.

[38] T.D. Fornes, P.J. Yoon, H. Keskkula, D.R. Paul, Nylon 6 nanocomposites: the effect of matrix molecular weight, Polymer 42 (2001) 9929-9940.

[39] D. Chu, Q. Nguyen, D. G. Baird, Effect of Matrix Molecular Weight on the Dispersion of Nanoclay in Unmodified High Density Polyethylene, Polym. Compos. (2007) 499-511.

[40] E. Abraham, B. Deepa, L. A. Pothan, M. John, S. S. Narine, S. Thomas, R. Anandjiwala, Physicomechanical properties of nanocomposites based on cellulose nanofibre and natural rubber latex, Cellulose 20 (2013) 417–427.

[41] M. J. Silva, A. O. Sanches, E. S. Medeiros, L. H. C. Mattoso, C. M. McMahan, J. A. Malmonge, Nanocomposites of natural rubber and polyaniline-modified cellulose nanofibrils, J. Therm. Anal. Calorim. 117 (2014) 387–392.

[42] T. H. S. Maia, N. M. Larocca, C. A. G. Beatrice, A. J. de Menezes, G. de Freitas Siqueira, L. A. Pessan, A. Dufresne, M. P. Franc, A. de Almeida Lucas, Polyethylene cellulose nanofibrils nanocomposites, Carbohydr. Polym. 173 (2017) 50–56.

[43] A. O. Sanches, L. H. S. Ricco, L. F. Malmonge, M. J. da Silva, W. K. Sakamoto, J. A. Malmonge, Influence of cellulose nanofibrils on soft and hard segments of polyurethane/cellulose nanocomposites and effect of humidity on their mechanical properties, Polym. Test. 40 (2014) 99-105.

[44] S. Qian, K. Sheng, PLA toughened by bamboo cellulose nanowhiskers: Role of silane compatibilization on the PLA bionanocomposite properties, Composites Science and Technology 148 (2017) 59-69.